Increased Ion Conductivity in Composite Solid Electrolytes With Porous Co$_3$O$_4$ Cuboids

Qiongyu Zhou[1,2]*, Songli Liu[2]*, Shiju Zhang[3], Yong Che[4] and Li-Hua Gan[1]*

[1]School of Chemistry and Chemical Engineering, Southwest University, Chongqing, China, [2]Chongqing Key Laboratory of Inorganic Special Functional Materials, College of Chemistry and Chemical Engineering, Yangtze Normal University, Chongqing, China, [3]College of Vanadium and Titanium, Panzhihua University, Panzhihua, China, [4]Enpower Energy (Anhui) Corp.y, Hefei, China

Compared with the fagile ceramic solid electrolyte, Li-ion conducting polymer electrolytes are flexible and have better contact with electrodes. However, the ionic conductivity of the polymer electrolytes is usually limited because of the slow segment motion of the polymer. In this work, we introduce porous Co$_3$O$_4$ cuboids to Poly (Ethylene Oxide)-based electrolyte (PEO) to investigate the influence of these cuboids on the ionic conductivity of the composite electrolyte and the performance of the all-solid-state batteries. The experiment results showed the porous cuboid Co$_3$O$_4$ fillers not only break the order motion of segments of the polymer to increase the amorphous phase amount, but also build Li$^+$ continuous migration pathway along the Co$_3$O$_4$ surface by the Lewis acid-base interaction. The Li$^+$ conductivity of the composite polymer electrolyte reaches 1.6×10^{-4} S cm^{-1} at 30°C. The good compatibility of the composite polymer electrolyte to Li metal anode and LiFePO$_4$ cathode ensures good rate performance and long cycle life when applying in an all-solid-state LiFePO$_4$ battery. This strategy points out the direction for developing the high-conducting composite polymer electrolytes for all-solid-state batteries.

Keywords: polymer electrolyte, all-solid-state battery, porous cuboid, hydrothermal method, surface interaction

INTRODUCTION

The demand for energy storage in today's technological society is increasing rapidly (Chen et al., 2009; Luo et al., 2015). With the exhaustion of fossil fuels and the increasingly severe environmental problems, it has become a worldwide trend to seek green, clean, and renewable energy (Abada et al., 2016). Lithium-ion batteries have been widely used in various portable smart devices since commercialized by Sony in 1991 (Thackeray et al., 2012). However, the capacity density of the commercial lithium-ion batteries with graphitized carbon anode can no longer meet the demand of electric vehicles (Lu et al., 2013; Cheng et al., 2017). Meanwhile, the flammable characteristic of the liquid electrolyte makes battery safety accidents frequently occur (Doughty and Roth, 2012).

An all-solid-state battery with a lithium metal anode due to its improved energy density and safety characteristic is a strong candidate for higher power and energy density in electrified transport (Lee et al., 2020). In order to ensure the long-term stable cycle of all-solid-state lithium metal batteries, the solid-state electrolyte (SSE) needs to have high Li$^+$ conductivity, good stability with the electrode, and the ability to block lithium dendrites (Goodenough and Singh, 2015). Much progress has been made in the study of inorganic SSEs. The oxide SSEs including garnet (Li et al., 2012; Thangadurai et al.,

2014; Li et al., 2018a), perovskite (Li et al., 2018b), and NASICON (Li et al., 2016) with Li$^+$ conductivity of 10^{-5}–10^{-3} S cm^{-1}, large electrochemical window, and certain mechanical strength were thought to be ideal SSEs. However, the high sintering temperature, high cost, and difficulty in mass production make them difficult for industrial application (Thangadurai et al., 2014). The sulfide SSEs and halide SSEs have higher Li$^+$ conductivity than liquid electrolytes, but most of them are unstable with lithium metal, and their narrow electrochemical window limits their development in all-solid-state batteries (Sakuda et al., 2013; Hayashi et al., 2016; Park et al., 2020).

Polymer solid electrolytes have attracted the attention of researchers because of their low cost and easy preparation (Stephan and Nahm, 2006; Wu et al., 2020a). Poly(ethylene oxide) (PEO), which is cheap and flexible, has become one of the most common polymer matrices of polymer solid electrolytes. However, even with the addition of lithium salt, the crystalline PEO phase always exists in PEO/Li-salt polymers, leading to low Li-ion conductivity of about 10^{-6} S cm^{-1} (Marzantowicz et al., 2006). Improving the Li$^+$ conductivity of the polymer solid electrolytes is the key point of their practical application. Adding fillers to the polymer is an effective strategy for improving the Li$^+$ conductivity of the electrolytes (Yue et al., 2016). By adding oxide fillers such as Al$_2$O$_3$, SiO$_2$, and TiO$_2$ to the polymer, on the one hand, these oxide particles can interrupt the ordered movement of the polymer chain segments and increase the content of the amorphous phase (Weston and Steele, 1982; Sabrina et al., 2019). On the other hand, the O/OH groups on the surface of the particles can produce Lewis acid-base interaction with lithium salt ions, which further promotes the transport of lithium ions in the composite solid electrolytes (Jayathilaka et al., 2002). Based on this, the main goal of this experiment is to prepare a filler with a large specific surface area that can absorb a large number of O/OH groups and provide a long-term pathway for continuous conduction of lithium ions.

In this study, porous cuboid Co$_3$O$_4$ was prepared by the hydrothermal method with subsequent heat treatment. Adding porous cuboid Co$_3$O$_4$ to PEO/LiTFSI increases the content of the amorphous phase of PEO. Meanwhile, the porous surface of Co$_3$O$_4$ can absorb a large number of O/OH groups so that lithium ions can also be transported along the surface of the Co$_3$O$_4$ cuboid. The Li$^+$ conductivity of the composite polymer electrolyte reaches 1.6×10^{-4} S cm^{-1} at 30°C. Moreover, the all-solid-state lithium/LiFePO$_4$ battery employing the electrolyte shows good rate performance and cycle stability at 40°C.

EXPERIMENTAL

Preparation of the Porous Cuboid Co$_3$O$_4$

The porous cuboid Co$_3$O$_4$ was prepared via the hydrothermal method with subsequent heat treatment. 1 mmol cobalt acetate tetrahydrate (Co(CH$_3$COO)$_2$•4H$_2$O, ACROS Organics) was dissolved in 18 ml ethanol and acetic acid composite solvent. The volume ratio of the ethanol and acetic acid was 3:1. The homogeneous solution was transferred into a 25 ml polytetrafluoroethylene (PTFE) liner and sealed in a stainless

steel reaction kettle. After heating at 180°C in an oven for 3 h, the precipitate was washed using ethanol and dried at 80°C. The porous cuboid Co$_3$O$_4$ was obtained by sintering the precursor in a box furnace at 350°C for 1 h.

Preparation of the Composite Polymer Electrolyte

Polyethylene oxide (PEO, M.W. ~600,000, ACROS Organics) and Lithium bis (trifluoromethanesulfonyl) imide (LiTFSI, ACROS Organics) were dried at 60°C overnight before use. The dried PEO and LiTFSI were added into anhydrous acetonitrile with the [EO] and [Li$^+$] molar ratio of 10:1. After stirring at 60°C for 12 h, the porous cuboid Co$_3$O$_4$ was added into the solution under vigorous stirring. The composite polymer electrolyte (CPE) was obtained by pouring the homogeneous mixture onto a PTFE plate and drying vacuumed at 60°C for 24 h. According to the weight percentage (5, 10, and 20 wt%) of the porous cuboid Co$_3$O$_4$, the CPEs were named CPE-5, CPE-10, and CPE-20, respectively.

A CPE using purchased Co$_3$O$_4$ (Alfa Aesar) as the filler was prepared using the method mentioned above. The sample was named CPE-purchased Co$_3$O$_4$.

Characterization

The phase and the morphology of the porous cuboid Co$_3$O$_4$ and the CPEs are characterized by an X-ray diffractometer (XRD, Rigaku MiniFlex 600), and a scanning electron microscope (SEM, FEI Quanta 650) equipped Bruker energy-dispersive X-ray spectroscopy (EDX) system.

The Li$^+$ conductivity (σ) of the CPEs is calculated by **Eq. 1**,

$$\sigma = \frac{l}{RA}, \tag{1}$$

where l, R, and A correspond to the thickness, impedance, and surface area of the CPEs, respectively. The electrochemical impedance spectroscopy (EIS) of the CPEs is tested by an Autolab workstation using a stainless steel/CPE/stainless steel coin cell, in which the stainless steel is used as the blocking electrode. The frequency is set as 10^6 to 0.1 Hz.

The Flourier transform infrared (FTIR) spectra of the CPEs are characterized by an Infinity Gold FTIR spectrometer from 400 to 4,000 cm^{-1}.

The differential scanning calorimetry curves (DSC) of the CPEs are recorded at the temperature range −80 to 0°C with a heating rate of 10°C min^{-1}.

To calculate the Li$^+$ transference number (t_{Li}^+) of the CPEs, the Li/CPE/Li battery is applied a dc voltage (ΔV, 10 mV here) until getting a steady current. The t_{Li}^+ is calculated according to **Eq. 2**,

$$t_{Li}^+ = \frac{I_s R'_b (\Delta V - I_0 R_i)}{I_0 R_b \left(\Delta V - I_s R'_i \right)}, \tag{2}$$

where I_0 and I_s are the initial and steady-state current, R_b and R'_b are the bulk resistances before and after applying the ΔV, R_i and R'_i are the interfacial resistances before and after the dc polarization.
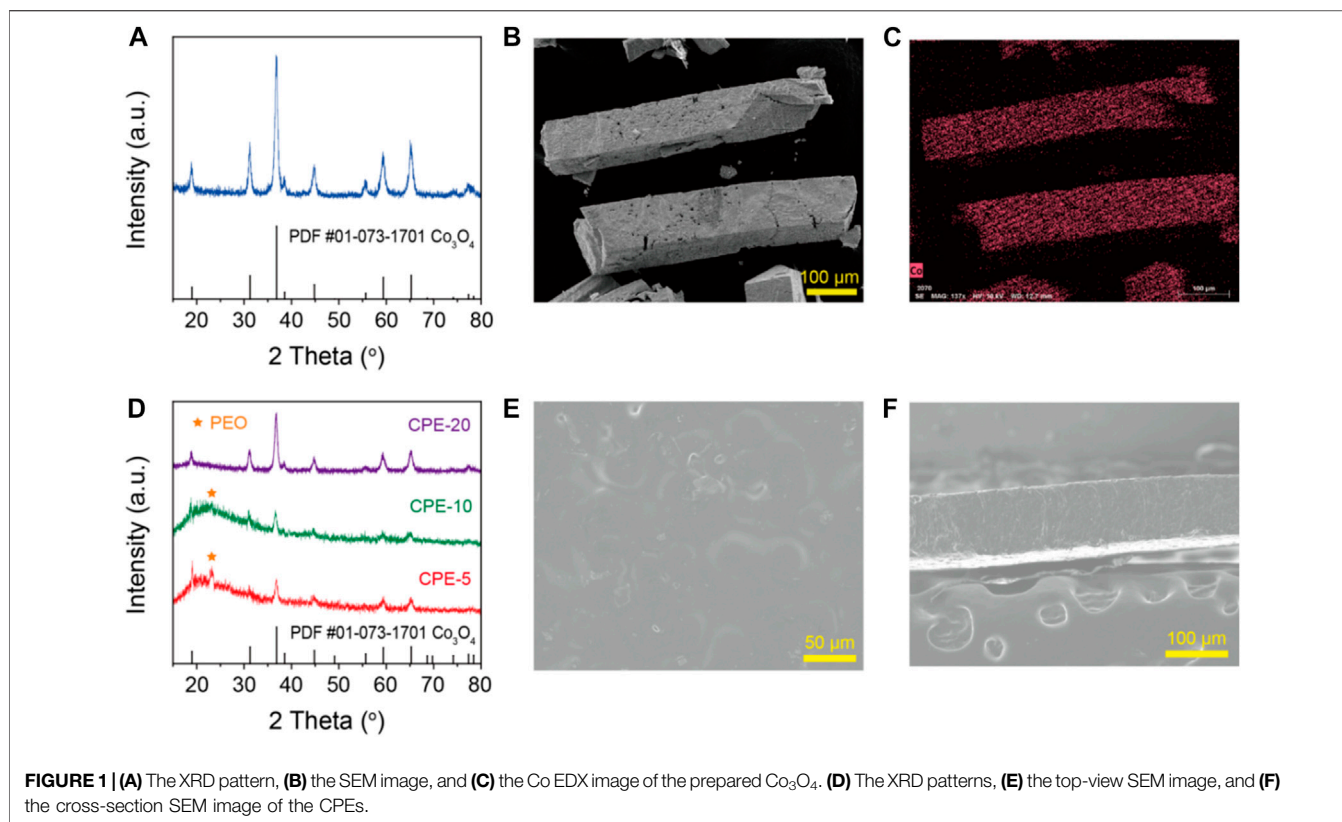
FIGURE 1 | (A) The XRD pattern, **(B)** the SEM image, and **(C)** the Co EDX image of the prepared Co$_3$O$_4$. **(D)** The XRD patterns, **(E)** the top-view SEM image, and **(F)** the cross-section SEM image of the CPEs.
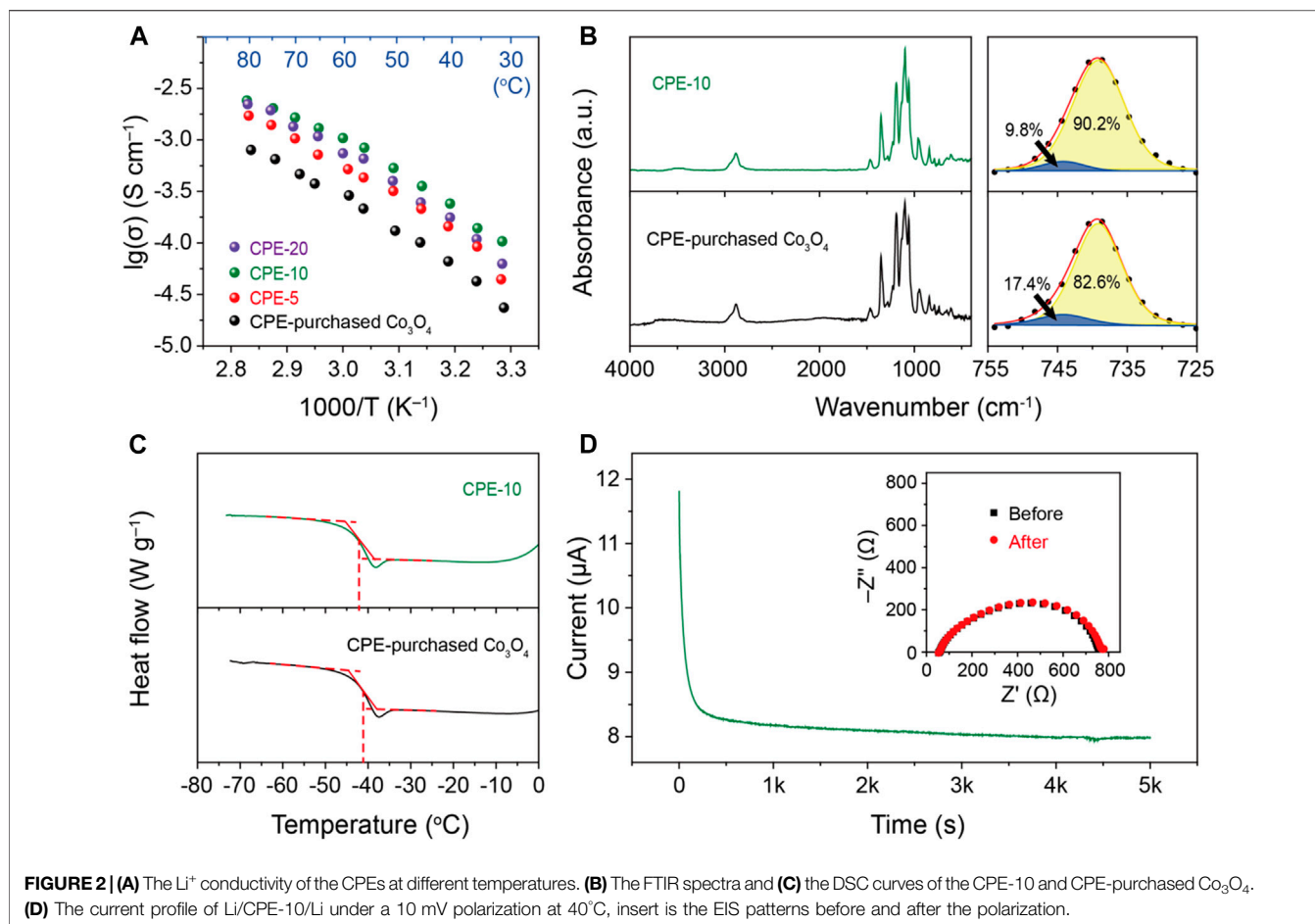
The solid-state LiFePO$_4$ cathode is prepared by mixing the LiFePO$_4$, PEO, LiTFSI, and carbon black (60:20:10:10 in weight ratio) into anhydrous acetonitrile. After stirring at 60°C for 12 h, the slurry was cast onto a carbon-coated aluminum foil. The LiFePO$_4$ cathode is obtained by drying in a vacuum at 60°C for 24 h.

RESULTS AND DISCUSSION

The XRD pattern of the prepared Co$_3$O$_4$ was shown in **Figure 1A**. All the diffraction peaks correspond well with the Co$_3$O$_4$ standard PDF card (#01-073-1701). No impurity phase is observed. As can be seen from **Figures 1B,C**, the prepared Co$_3$O$_4$ shows a porous cuboid structure. The ethanol and acetic acid composite solvent promote the orientation growth of the Co$_3$O$_4$. The side length and the height of the cuboid are approximately 100 and 550 μm, respectively. The XRD patterns of the CPEs with different addition of porous cuboid Co$_3$O$_4$ were given in **Figure 1D**. The diffraction peaks of the Co$_3$O$_4$ show no change in each CPEs, which means the Co$_3$O$_4$ is chemical stable with PEO and LiTFSI. An obvious crystalline peak of PEO exits at 23° in the XRD pattern of the CPE with 5 wt% Co$_3$O$_4$. When adding 10 wt% Co$_3$O$_4$, the intensity of the PEO crystalline peak becomes weak. And the PEO crystalline peak is invisible in the CPE-20. The amorphous degree of the composite polymer could be increased by adding porous cuboid Co$_3$O$_4$ as the fillers, which facilitates the movement of Li$^+$ in the CPEs. The CPEs are dense and have a flat surface (**Figure 1E**). The thickness of the CPEs is controlled at 100 μm (**Figure 1F**). As can be seen from the top-view and cross-section SEM images (**Figures 1E,F**), the Co$_3$O$_4$ cuboids are uniformly dispersed in the polymer.

The temperature-dependent Li$^+$ conductivity of the CPEs with different addition of the porous cuboid Co$_3$O$_4$ are shown in **Figure 2A**. With the increase of the addition amount of the porous cuboid Co$_3$O$_4$, the Li$^+$ conductivity increases first and then decreases. The CPE with 10 wt% porous cuboid Co$_3$O$_4$ shows the highest Li$^+$ conductivity among the CPEs, which is 1.6×10^{-4} S cm^{-1} at 30°C. When the weight percentage of the porous cuboid Co$_3$O$_4$ is 20 wt%, the Li$^+$ transport path may be blocked by excess Co$_3$O$_4$ in the polymer, leading to a slight decrease of the Li$^+$ conductivity (Dissanayake et al., 2003). 10 wt% commercial Co$_3$O$_4$ powders were added into the PEO/LiTFSI as the fillers for comparison. Unlike the prepared Co$_3$O$_4$, the purchased Co$_3$O$_4$ is nearly spherical in morphology (**Supplementary Figure S1A**). The Li$^+$ conductivity of the CPE-purchased Co$_3$O$_4$ (2.0×10^{-5} S cm^{-1} at 30°C), which is of the same order of magnitude as that of CPEs using other Li-insulator oxide fillers such as Al$_2$O$_3$ or TiO$_2$ (Croce et al., 1998), is much lower than that of CPEs with porous cuboid Co$_3$O$_4$. In order to figure out the reason why the Li$^+$ conductivity of the CPE-10 is much higher than that of the CPE-purchased Co$_3$O$_4$, the FTIR spectra of the two membranes are compared in **Figure 2B**. Overall, the FTIR spectra of the CPEs with different morphologies show very similar peak positions and relative intensities. After fitting the peaks in the range of
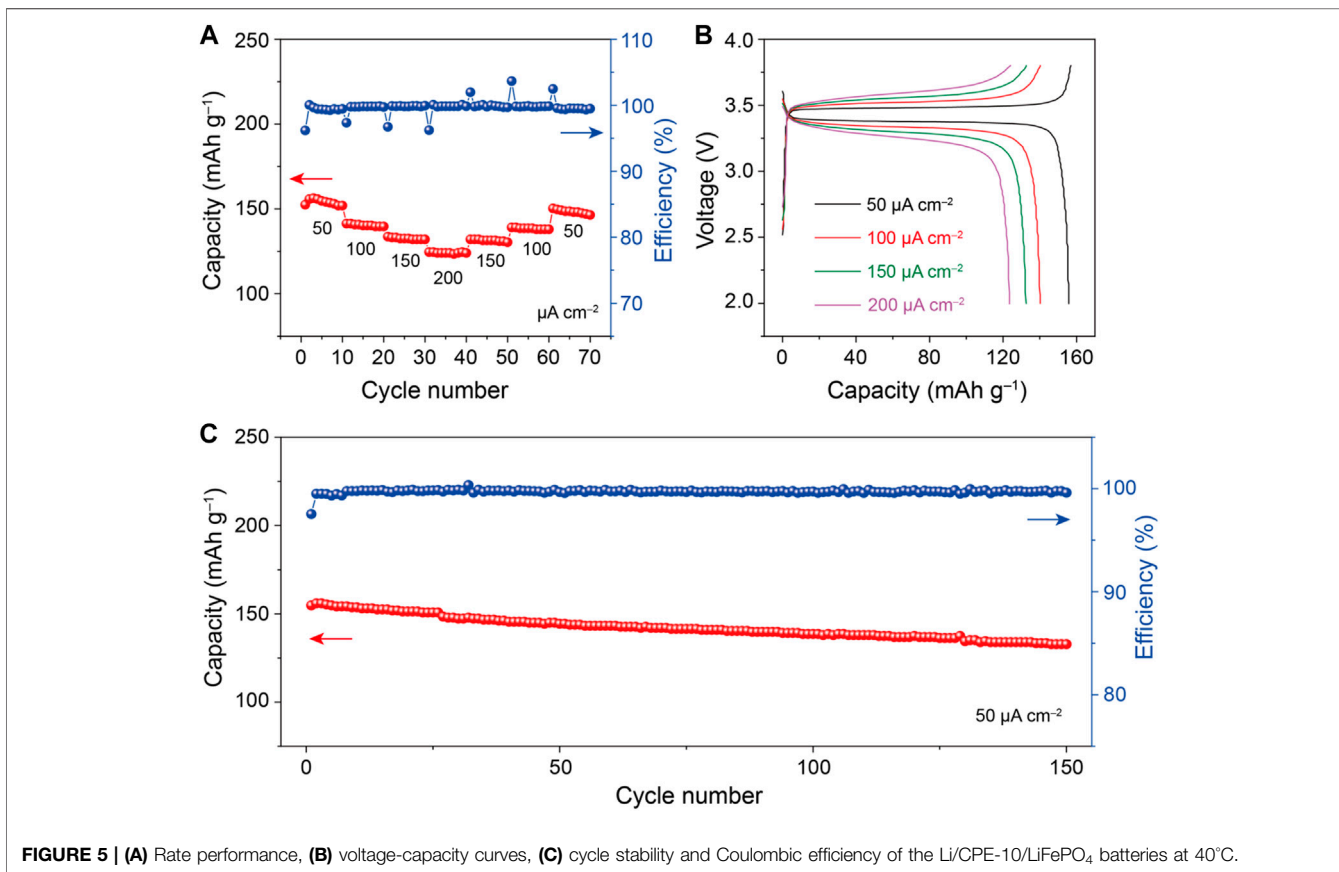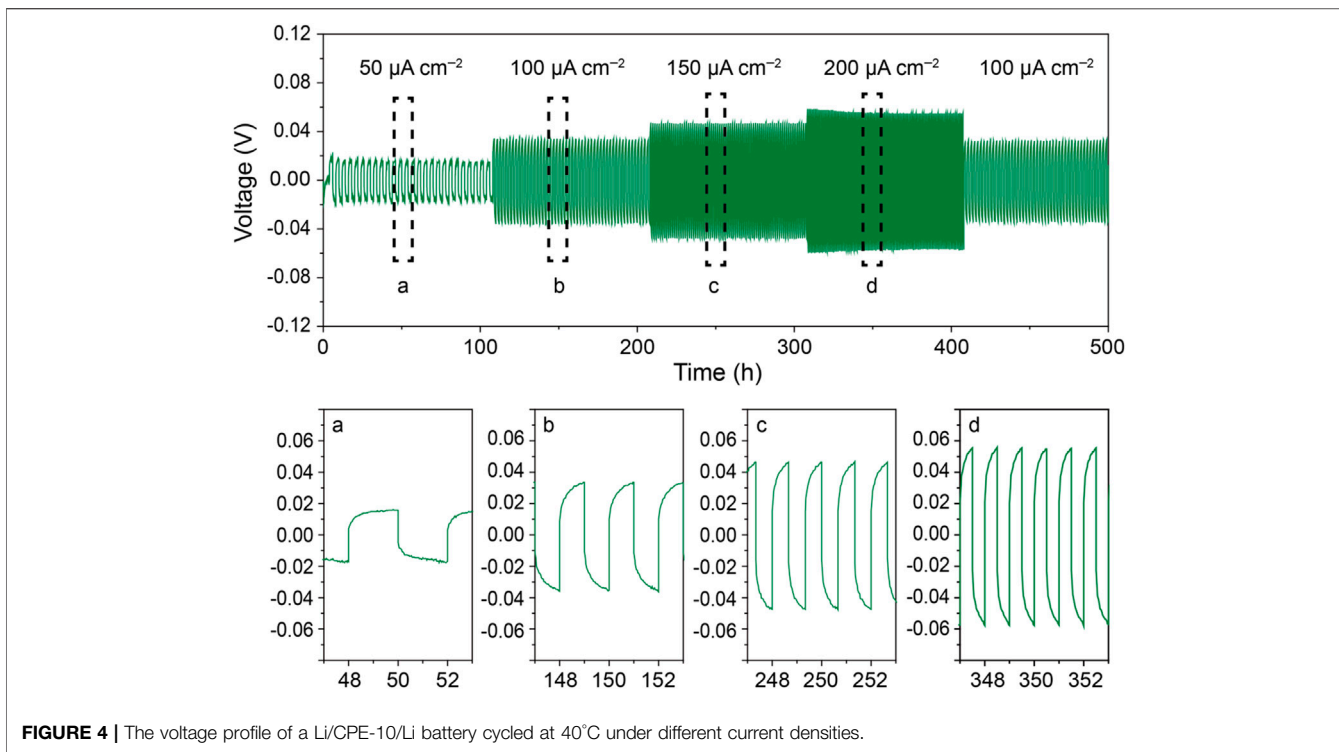
FIGURE 2 | (A) The Li$^+$ conductivity of the CPEs at different temperatures. (B) The FTIR spectra and (C) the DSC curves of the CPE-10 and CPE-purchased Co_3O_4. (D) The current profile of Li/CPE-10/Li under a 10 mV polarization at 40°C, insert is the EIS patterns before and after the polarization.

725~755 cm^{-1}, it is worth noting that 90.2% of the lithium salt is dissociated in PEO, forming free Li$^+$ and TFSI$^-$ (corresponding to the yellow peak centered at about 739 cm^{-1}) in the CPE-10. However, in the CPE-purchased Co_3O_4, there are fewer free cations/anions (82.6%), but 17.4% of ion-paired LiTFSI (corresponding to the blue peak centered at about 744 cm^{-1}), which has no contribution to the Li$^+$ transport (Bakker et al., 1995; Wu et al., 2020b). From the DSC curves of the CPE-10 and the CPE-purchased Co_3O_4 in **Figure 2C**, the glass transition temperature (T_g) of the CPE-10 and the CPE-purchased Co_3O_4 are −42.3 and −40.8°C, respectively. The lower T_g of the CPE-10 means that the porous cuboid Co_3O_4 as fillers have a better impact on inhibiting the crystallization of PEO polymer and promoting the movement of the molecular chains compared to the purchased Co_3O_4. Moreover, the Li$^+$ transference number of the CPE-10 is calculated as 0.28 (**Figure 2D**), which is much higher than that of the CPE-purchased Co_3O_4 (0.13 as shown in **Supplementary Figure S2**). The higher Li$^+$ transference number of the CPE-10 could reduce the concentration polarization during cell cycling and fulfill a long-term cycle life when employing in an all-solid-state battery.

The Li$^+$ conductivity of a CPE could be improved by adding Li-insulator oxide fillers into PEO/LiTFSI for two reasons. Firstly, oxides dispersed in the PEO/LiTFSI matrix could break the ordered arrangement of PEO chain segments, thus decrease

FIGURE 3 | The schematic diagram of the Li$^+$ transport paths in the CPE-10 and CPE-purchased Co_3O_4.
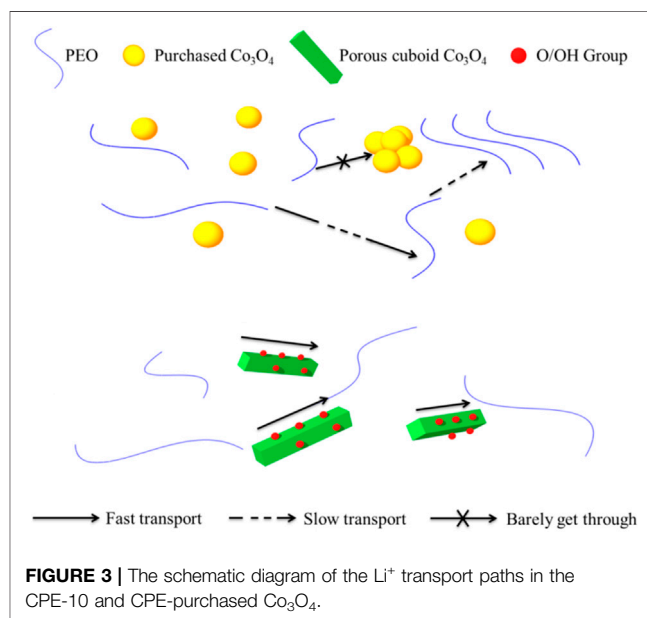
the crystalline amount and inhibit the re-crystallization. Secondly, the Lewis acid-base type O/OH groups on the filler surface could interact with cations and anions to create high

FIGURE 4 | The voltage profile of a Li/CPE-10/Li battery cycled at 40°C under different current densities.

FIGURE 5 | (A) Rate performance, (B) voltage-capacity curves, (C) cycle stability and Coulombic efficiency of the Li/CPE-10/LiFePO$_4$ batteries at 40°C.

conducting Li$^+$ pathways[24, 25]. The transport paths of Li$^+$ in the CPE-10 and the CPE-purchased Co$_3$O$_4$ are shown in **Figure 3**. The Co$_3$O$_4$ particles are easy to agglomerate (**Supplementary Figure S1B**), resulting in uneven distribution when adding into the PEO/LiTFSI matrix. Li$^+$ cannot pass through agglomerate particles. Li$^+$ transfer will slow down in the crystalline area due to a lack of fillers. On the contrary, in the homogeneous CPE-10, Li$^+$ moves fast through the PEO segments and the Co$_3$O$_4$ porous cuboids. What's more, lots of O/OH groups are absorbed on the Co$_3$O$_4$ porous surfaces (Yan and Sautet, 2019; Chen et al., 2020). The Li$^+$ cation in the LiTFSI is quite a strong Lewis acid (the TFSI$^-$ anion is a Lewis base). The surface O/OH groups will absorb cations and anions, respectively, by Lewis acid-base interaction, promoting the dissociation of the lithium and the movement of the ions (Wieczorek et al., 1996). The Lewis acid-base interaction between O/OH groups and ions could create continuous, long-term Li$^+$ transport paths along the Co$_3$O$_4$ porous cuboid surface, leading to an increase in Li$^+$ conductivity.

To determine the electrochemical properties of the CPE-10, all-solid-state Li/Li and Li/LiFePO$_4$ batteries were assembled using the CPE-10 as the electrolyte. The voltage profile of the Li/CPE-10/Li battery cycled at 40°C under different current densities is shown in **Figure 4**. The battery exhibits excellent cycle stability under 50–200 µA cm^{-2} for 500 h. The polarization is 0.018, 0.034, 0.048, and 0.057 V when current density is 50, 100, 150, and 200 µA cm^{-2}, respectively. After current density decreasing back to 100 µA cm^{-2}, the voltage recovers to 0.039 V. No sudden increase or drop in voltage polarization was observed, indicating a stable interface between the Li metal and the CPE-10.

All-solid-state Li/CPE-10/LiFePO$_4$ batteries were cycled at 40°C to evaluate the practical possibilities of the CPE-10. As can be seen from **Figure 5A**, the discharge capacity of the battery is about 155, 140, 132, and 126 mAh g^{-1} when current density increases from 50 to 200 µA cm^{-2}, and the discharge capacity recovers to 132, 139, and 150 mAh g^{-1} when the current density is 150, 100, and 50 µA cm^{-2}, respectively. The outstanding rate performance and tiny voltage polarization (**Figure 5B**) demonstrates that the electrodes and electrolyte have good compatibility. Based on it, a Li/CPE-10/LiFePO$_4$ battery was cycled under 50 µA cm^{-2} at 40°C to estimate the cycle life of the battery (**Figure 5C**). After 150 cycles, the discharge capacity is 132 mAh g^{-1}. The capacity retention is high as 83%. The Coulombic efficiency keeps over 98% during the long cycle life. The good rate performance and long cycle life prove that the low-cost electrolyte has a promising application in all-solid-state lithium metal batteries.

CONCLUSION

The porous cuboid Co$_3$O$_4$ fillers, which are synthesized via the hydrothermal method, is added into the PEO/LiTFSI to prepare a composite polymer electrolyte. The porous cuboid Co$_3$O$_4$ fillers not only break the order motion of segments of the polymer to increase the amorphous phase amount, but also build Li$^+$ continuous migration pathway along the Co$_3$O$_4$ surface by the Lewis acid-base interaction. The Li$^+$ conductivity of the composite polymer electrolyte reaches 1.6×10^{-4} S cm^{-1} at 30 C. The good compatibility of the composite polymer electrolyte to Li metal anode and LiFePO$_4$ cathode ensures good rate performance and long cycle life when applying in an all-solid-state LiFePO$_4$ battery.

DATA AVAILABILITY STATEMENT

The original contributions presented in the study are included in the article/**Supplementary Material**, further inquiries can be directed to the corresponding authors.

AUTHOR CONTRIBUTIONS

QZ: experimental design, data analysis and discussion, and manuscript writing. SL and L-HG: experimental design and data analysis and manuscript writing. SZ and YC: electrochemical performance test. All authors contributed to the article and approved the submitted version.

FUNDING

SUPPLEMENTARY MATERIAL

The Supplementary Material for this article can be found online at: https://www.frontiersin.org/articles/10.3389/fmats.2021.697257/full#supplementary-material

REFERENCES

Abada, S., Marlair, G., Lecocq, A., Petit, M., Sauvant-Moynot, V., and Huet, F. (2016). Safety Focused Modeling of Lithium-Ion Batteries: A Review. *J. Power Sourc.* 306, 178–192. doi:10.1016/j.jpowsour.2015.11.100

Bakker, A., Gejji, S., Lindgren, J., Hermansson, K., and Probst, M. (1995). Contact Ion Pair Formation and Ether Oxygen Coordination in the Polymer Electrolytes M[N(CF3SO2)2]2PEOn for M = Mg, Ca, Sr and Ba. *Polymer* 36 (23), 4371–4378. doi:10.1016/0032-3861(95)96841-U

Chen, H., Cong, T. N., Yang, W., Tan, C., Li, Y., and Ding, Y. (2009). Progress in Electrical Energy Storage System: A Critical Review. *Prog. Nat. Sci.* 19 (3), 291–312. doi:10.1016/j.pnsc.2008.07.014

Chen, K., Li, W., Zhou, Z., Huang, Q., Liu, Y., and Duan, Q. (2020). Hydroxyl Groups Attached to Co2+ on the Surface of Co3O4: a Promising Structure for Propane Catalytic Oxidation. *Catal. Sci. Technol.* 10 (8), 2573–2582. doi:10.1039/D0CY00265H

Cheng, X.-B., Zhang, R., Zhao, C.-Z., and Zhang, Q. (2017). Toward Safe Lithium Metal Anode in Rechargeable Batteries: a Review. *Chem. Rev.* 117 (15), 10403–10473. doi:10.1021/acs.chemrev.7b00115

Croce, F., Appetecchi, G. B., Persi, L., and Scrosati, B. (1998). Nanocomposite Polymer Electrolytes for Lithium Batteries. *Nature.* 394 (6692), 456–458. doi:10.1038/28818

Dissanayake, M. A. K. L., Jayathilaka, P. A. R. D., Bokalawala, R. S. P., Albinsson, I., and Mellander, B.-E. (2003). Effect of Concentration and Grain Size of Alumina Filler on the Ionic Conductivity Enhancement of the (PEO)9LiCF3SO3:Al2O3 Composite Polymer Electrolyte. *J. Power Sourc.* 119-121, 409–414. doi:10.1016/s0378-7753(03)00262-3

Doughty, D. H., and Roth, E. P. (2012). A General Discussion of Li Ion Battery Safety. *Electrochem. Soc. Interf.* 21 (2), 37. doi:10.1149/2.F03122if

Goodenough, J. B., and Singh, P. (2015). Review-Solid Electrolytes in Rechargeable Electrochemical Cells. *J. Electrochem. Soc.* 162 (14), A2387–A2392. doi:10.1149/2.0021514jes

Hayashi, A., Sakuda, A., and Tatsumisago, M. (2016). Development of Sulfide Solid Electrolytes and Interface Formation Processes for Bulk-type All-Solid-State Li and Na Batteries. *Front. Energ. Res.* 4, 25. doi:10.3389/fenrg.2016.00025

Jayathilaka, P. A. R. D., Dissanayake, M. A. K. L., Albinsson, I., and Mellander, B.-E. (2002). Effect of Nano-Porous Al2O3 on thermal, Dielectric and Transport Properties of the (PEO)9LiTFSI Polymer Electrolyte System. *Electrochim Acta* 47 (20), 3257–3268. doi:10.1016/S0013-4686(02)00243-8

Lee, Y.-G., Fujiki, S., Jung, C., Suzuki, N., Yashiro, N., Omoda, R., et al. (2020). High-energy Long-Cycling All-Solid-State Lithium Metal Batteries Enabled by Silver-Carbon Composite Anodes. *Nat. Energ.* 5 (4), 299–308. doi:10.1038/s41560-020-0575-z

Li, Y., Chen, X., Dolocan, A., Cui, Z., Xin, S., Xue, L., et al. (2018a). Garnet Electrolyte with an Ultralow Interfacial Resistance for Li-Metal Batteries. *J. Am. Chem. Soc.* 140 (20), 6448–6455. doi:10.1021/jacs.8b03106

Li, Y., Han, J. T., Wang, C. A., Xie, H., and Goodenough, J. B. (2012). Optimizing Li+ Conductivity in a Garnet Framework. *J. Mater. Chem.* 22 (30), 15357–15361. doi:10.1039/C2JM31413D

Li, Y., Xu, H., Chien, P. H., Wu, N., Xin, S., Xue, L., et al. (2018b). A Perovskite Electrolyte that Is Stable in Moist Air for Lithium-Ion Batteries. *Angew. Chem. Int. Ed.* 57 (28), 8587–8591. doi:10.1002/anie.201804114

Li, Y., Zhou, W., Chen, X., Lü, X., Cui, Z., Xin, S., et al. (2016). Mastering the Interface for Advanced All-Solid-State Lithium Rechargeable Batteries. *Proc. Natl. Acad. Sci. USA.* 113 (47), 13313–13317. doi:10.1073/pnas.1615912113

Lu, L., Han, X., Li, J., Hua, J., and Ouyang, M. (2013). A Review on the Key Issues for Lithium-Ion Battery Management in Electric Vehicles. *J. Power Sourc.* 226, 272–288. doi:10.1016/j.jpowsour.2012.10.060

Luo, X., Wang, J., Dooner, M., and Clarke, J. (2015). Overview of Current Development in Electrical Energy Storage Technologies and the Application Potential in Power System Operation. *Appl. Energ.* 137, 511–536. doi:10.1016/j.apenergy.2014.09.081

Marzantowicz, M., Dygas, J. R., Krok, F., Nowiński, J. L., Tomaszewska, A., Florjańczyk, Z., et al. (2006). Crystalline Phases, Morphology and Conductivity of PEO:LiTFSI Electrolytes in the Eutectic Region. *J. Power Sourc.* 159 (1), 420–430. doi:10.1016/j.jpowsour.2006.02.044

Park, K.-H., Kaup, K., Assoud, A., Zhang, Q., Wu, X., and Nazar, L. F. (2020). High-voltage Superionic Halide Solid Electrolytes for All-Solid-State Li-Ion Batteries. *ACS Energ. Lett.* 5 (2), 533–539. doi:10.1021/acsenergylett.9b02599

Sabrina, Q., Sohib, A., Lestariningsih, T., and Ratri, C. R. (2019). The Effect of (TiO2 and SiO2) Nano-Filler on Solid Polymer Electrolyte Based LiBOB. *J. Phys. Conf. Ser.* 1191, 012028. doi:10.1088/1742-6596/1191/1/012028

Sakuda, A., Hayashi, A., and Tatsumisago, M. (2013). Sulfide Solid Electrolyte with Favorable Mechanical Property for All-Solid-State Lithium Battery. *Sci. Rep.* 3 (1), 1–5. doi:10.1038/srep02261

Stephan, A. M., and Nahm, K. S. (2006). Review on Composite Polymer Electrolytes for Lithium Batteries. *Polymer* 47 (16), 5952–5964. doi:10.1016/j.polymer.2006.05.069

Thackeray, M. M., Wolverton, C., and Isaacs, E. D. (2012). Electrical Energy Storage for Transportation-Approaching the Limits of, and Going beyond, Lithium-Ion Batteries. *Energy Environ. Sci.* 5 (7), 7854–7863. doi:10.1039/C2EE21892E

Thangadurai, V., Narayanan, S., and Pinzaru, D. (2014). Garnet-type Solid-State Fast Li Ion Conductors for Li Batteries: Critical Review. *Chem. Soc. Rev.* 43 (13), 4714–4727. doi:10.1039/C4CS00020J

Weston, J., and Steele, B. (1982). Effects of Inert Fillers on the Mechanical and Electrochemical Properties of Lithium Salt-Poly(ethylene Oxide) Polymer Electrolytes. *Solid State Ionics.* 7 (1), 75–79. doi:10.1016/0167-2738(82)90072-8

Wieczorek, W., Stevens, J. R., and Florjańczyk, Z. (1996). Composite Polyether Based Solid Electrolytes. The Lewis Acid-Base Approach. *Solid State Ionics.* 85 (1-4), 67–72. doi:10.1016/0167-2738(96)00042-2

Wu, N., Chien, P.-H., Li, Y., Dolocan, A., Xu, H., Xu, B., et al. (2020a). Fast Li+ Conduction Mechanism and Interfacial Chemistry of a NASICON/Polymer Composite Electrolyte. *J. Am. Chem. Soc.* 142 (5), 2497–2505. doi:10.1021/jacs.9b12233

Wu, N., Chien, P. H., Qian, Y., Li, Y., Xu, H., Grundish, N. S., et al. (2020b). Enhanced Surface Interactions Enable Fast Li + Conduction in Oxide/Polymer Composite Electrolyte. *Angew. Chem. Int. Ed.* 59 (10), 4131–4137. doi:10.1002/anie.201914478

Yan, G., and Sautet, P. (2019). Surface Structure of Co3O4 (111) under Reactive Gas-phase Environments. *ACS Catal.* 9 (7), 6380–6392. doi:10.1021/acscatal.9b01485

Yue, L., Ma, J., Zhang, J., Zhao, J., Dong, S., Liu, Z., et al. (2016). All Solid-State Polymer Electrolytes for High-Performance Lithium Ion Batteries. *Energ. Storage Mater.* 5, 139–164. doi:10.1016/j.ensm.2016.07.003